



26

Abstract

27 Utilizing a recent observational particulate matter with diameters less than 2.5 μm
28 ($\text{PM}_{2.5}$) dataset in North China, this study reveals a distinct seesaw feature of
29 abnormally high and low $\text{PM}_{2.5}$ concentrations in the adjacent two months of
30 December 2015 and January 2016, accompanied by distinct meteorological
31 modulations. The seesaw pattern is postulated to be linked to super El Niño and the
32 Arctic Oscillation (AO). During the mature phase of El Niño in December 2015, the
33 weakened East Asian Winter Monsoon (EAWM) and the associated low-level
34 southerly wind anomaly reduced planetary boundary layer height, favoring strong
35 haze formation. This circulation pattern was completely reversed in the following
36 month, in part due to a sudden phase change of the AO from positive to negative and
37 the beginning of a decay of the El Niño, which enhanced the southward shift of the
38 upper-tropospheric jet from December to January relative to climatology, leading to
39 an enhanced EAWM and substantially lower haze formation. This sub-seasonal
40 change in circulation is also robustly found in 1982/1983 and 1997/1998, implicative
41 of a general physical mechanism dynamically linked to El Niño and the AO.
42 Numerical experiments with the Weather Research and Forecasting
43 (WRF)-Community Multi-scale Air Quality (CMAQ) model were used to test the
44 modulation of the meteorological conditions on haze formation. With the same
45 emission, simulations for three super El Niño periods (1983, 1997 and 2015) robustly
46 show higher $\text{PM}_{2.5}$ concentrations under the mature phase of the super El Niño, but
47 substantially lower $\text{PM}_{2.5}$ concentrations during the decay phase of El Niño (and the
48 sudden AO phase change), further verifying the modulation effect of sub-seasonal
49 circulation anomaly on $\text{PM}_{2.5}$ concentrations in North China.

50 **Key words:** Haze, El Niño, Arctic Oscillation, East Asian winter monsoon,
51 WRF/CMAQ

52



53 1. Introduction

54 China has experienced severe haze pollution in recent years (Tie et al., 2017; Ding
55 et al., 2016; Zhang et al., 2015; Song et al., 2017), with potentially detrimental effect
56 on human health (Chen et al., 2017) as suggested by a substantial increase in hospital
57 visits during the haze season (Liang et al., 2017; Xu et al., 2017c). Understanding the
58 mechanism of haze formation is vital for developing effective measures to relieve the
59 haze pollution. Despite the continued reduction in anthropogenic emission such as
60 NO_x, SO₂, and CO in China in the past few years (Liu et al., 2016; Li et al.,
61 2017; Wang et al., 2017), the severe haze pollution motivates a need to understand the
62 mechanism of haze formation from a meteorological perspective (He et al., 2017; Ding
63 et al., 2016). A few studies investigated the relationship between haze and climate
64 variability at decadal or longer time scales (Xu et al., 2017a; Yin et al., 2017; Jeong and
65 Park, 2017; Zhang et al., 2016; Liu et al., 2017; Wu et al., 2015), while others examined
66 the meteorological factors associated with specific severe haze events (Yin et al.,
67 2017; Cai et al., 2017b; Li et al., 2018).

68 By using a long-term observational data set from 1972-2014, Li et al. (2016)
69 found that the number of fog-haze days in winter across central and eastern China has
70 a strong relationship with the East Asian winter monsoon (EAWM), with weak
71 EAWM favoring the accumulation of haze by weakening the near surface wind speed.
72 This effect was further illustrated by Yang et al. (2016) using a twenty-year long
73 simulation from 1985 to 2005 with the Goddard Earth-Observing System chemical
74 transport model (GEOS-Chem). Zooming in on the severe haze event in 2013, Cai et
75 al. (2017b) identified the conducive weather conditions for severe haze including
76 weakened surface northerlies and northward shift of mid-troposphere northwesterlies
77 extending to the north of Beijing, reducing the cold and dry flow to Beijing.

78 The recent severe haze event in December 2015 has been linked to the strong El
79 Niño condition (Zhang et al., 2017; Chang et al., 2016; Yuan et al., 2017). For example,
80 Yuan et al. (2017) investigated the impact of El Niño on the severe haze during



81 November to December of 2015 and found unfavorable meteorological conditions
82 during this period including a weak East Asian winter monsoon, reduced cold air
83 intrusion, decreased low level wind speed and enhanced stability unfavorable for
84 ventilation of pollutants. Similar to El Niño-Southern Oscillation (ENSO) but from a
85 decadal simulation, Zhao et al. (2016) found that the decadal variations of haze days
86 in central-eastern China during 1959–2012 are tightly associated with the Pacific
87 Decadal Oscillation (PDO), with more haze days occurring during positive PDO
88 phase, primarily resulting from enhancement of the Mongolia High and a stable
89 atmosphere, whereas an opposite effect was observed during the negative phase of
90 PDO. The modulation of El Niño on other air pollutants such as ozone has also been
91 investigated. For example, Xu et al. (2017b) found different effects of ENSO
92 modulation on ozone between the developing and decaying phase of ENSO. During
93 the developing phase in fall, El Niño tends to reduce ozone in the southeastern US
94 compared to La Niña, possibly due to the increased water vapor as an ozone sink and
95 cooler surface air temperature and stagnation. In contrast, during the decaying phase
96 in spring, ozone in the western US shows some decreases likely linked to the
97 decreased temperature and enhanced water vapor in that region.

98 While it is highly possible that the severe haze pollution in November to
99 December of 2015 is a result of the strong El Niño, the sudden drop in $PM_{2.5}$
100 concentrations in January 2016 compared to December 2015 has heretofore largely
101 been ignored. Puzzled by the seesaw pattern of severe haze pollution in December
102 2015 and the low $PM_{2.5}$ concentrations in January 2016, this study aims to explore the
103 possible mechanism behind this temporal seesaw phenomenon. The paper is
104 organized as follows. In Section 2, we introduce the data and methodology used in the
105 study, followed by the monthly variations of $PM_{2.5}$ concentration. In Section 4,
106 mechanisms regarding the haze variations are investigated.

107 **2. Data and methodology**

108 Meteorological data including zonal and meridional wind at 500 hPa and 850



109 hPa, geopotential height at 500 hPa, 2-m air temperature and planetary boundary layer
110 height, are from the European Centre for Medium-Range Weather Forecasts
111 (ECMWF) Interim Reanalysis Data (ERA-Interim) (Dee et al., 2011), with a spatial
112 resolution of 1.125° by 1.125°. Six hourly data were downloaded to calculate monthly
113 and daily mean. A thirty-year period of 1987-2016 is selected as the reference period
114 when anomaly is calculated. The AO index and Niño 3.4 index are available at the
115 Climate Prediction Center (CPC) website (<http://www.cpc.ncep.noaa.gov/>).

116 The PM_{2.5} hourly concentrations during 2014-2017, the only period with
117 available data, were downloaded from <http://www.pm25.in> for more than 1000
118 stations and the data were interpolated to the same spatial resolution as the
119 ERA-Interim, i.e., 1.125° by 1.125°. A longer-term dataset of PM_{2.5} concentrations
120 from 2009-2017 at the U.S. Embassy in Beijing (117°E, 40°N), was downloaded from
121 <http://www.stateair.net/web/historical/1/1.html>.

122 A regional meteorological model, Weather Research and Forecasting (WRF)
123 (Skamarock et al., 2008) model, coupled to a chemistry model, Community
124 Multi-scale Air Quality (CMAQ), was used to investigate possible factors modulating
125 haze formation. WRF version 3.8.1 was used in this study, with physics options same
126 as those discussed in Gao et al. (2017). The initial and boundary conditions for WRF
127 were provided by the NCEP Climate Forecast System Reanalysis (CFSR) version 2
128 (Saha et al., 2013), with a spatial resolution of 0.5 deg×0.5 deg. For regional chemistry,
129 the widely used CMAQ model (Byun and Ching, 1999;Byun and Schere, 2006), with
130 the latest version 5.2, was used in this study, with the carbon-bond version 6 (CB06) for
131 the major gas phase chemistry and AERO6 for aerosol module. The latest version of
132 Meteorology-Chemistry Interface Processor (MCIP 4.3) was used to post-process
133 WRF results and prepare input data for CMAQ (Otte and Pleim, 2010).The initial and
134 boundary chemical conditions were derived from Model for Ozone and Related
135 chemical Tracers, version 4 (MOZART-4). Downscaling from MOZART to CMAQ
136 was developed and discussed in detail in an upcoming paper (Ma et al., in preparation).



137 The emissions of air pollutants in China were estimated by Tsinghua University (Zhao
138 et al., 2013c; Zhao et al., 2013a; Wang et al., 2014; Cai et al., 2017a; Zhao et al., 2017)
139 using an “emission factor method”. The provincial emissions from area and mobile
140 sources were calculated from the activity data (energy consumption, industrial
141 product yields, solvent use, etc.), technology-based uncontrolled emission factors, and
142 penetrations of control technologies, and subsequently distributed to the model grids
143 according to the spatial distribution of population, GDP, and road networks. A
144 unit-based method is applied to estimate and locate the emissions from large point
145 sources including power plants, iron and steel plants, and cement plants. The biomass
146 burning emissions include open burning of agricultural residue, calculated based on
147 crop yields, fraction of biomass burned in the open field, etc (Fu et al., 2013; Zhao et
148 al., 2013b; Wang and Zhang, 2008). The emissions from natural forest and grassland
149 fires was ignored in this study, primarily due to the relatively small contribution in
150 particular over the North China (Qin and Xie, 2011). Biogenic emissions were
151 calculated by the Model of Emissions of Gases and Aerosols from Nature (MEGAN;
152 Guenther et al., 2006). For each month of the CMAQ simulations, a week of model
153 spin up was used to reduce the influence of the initial conditions.

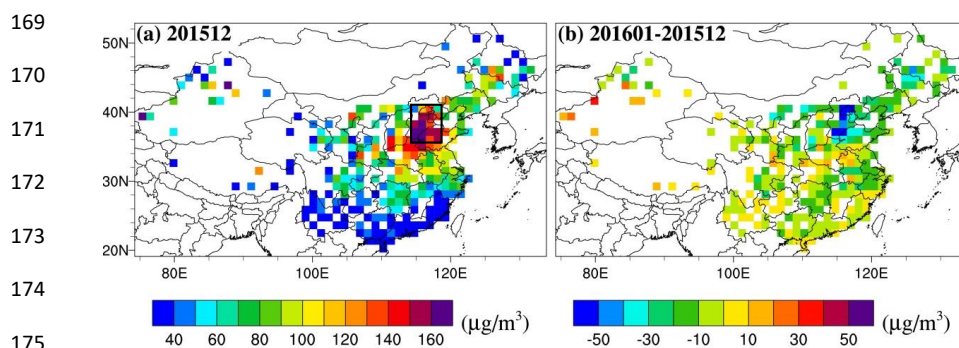
154 **3. Monthly variations of PM_{2.5} concentration**

155 3.1 Difference of PM_{2.5} in December 2015 and January 2016

156 Fig. 1 shows the spatial distribution of PM_{2.5} concentration in December 2015 (Fig.
157 1a) and the monthly mean difference between the anomaly of January 2016 (relative
158 to January from 2015-2017) and December 2015 (relative to December from
159 2014-2016). Consistent with previous studies (Zhang et al., 2017; Chang et al.,
160 2016; Yuan et al., 2017), severe haze pollution occurred in December 2015 particularly
161 over the North China Plain (NCP) (black box in Fig. 1a), with monthly mean PM_{2.5} as
162 high as 148 µg/m³, much higher than that in December 2014 (97 µg/m³) and slightly
163 higher than that in December 2016 (135 µg/m³). In January 2016, the anomaly
164 (relative to January from 2015-2017) of PM_{2.5} showed large decrease compared to the



165 anomaly of December 2015 (relative to December from 2014-2016) over the NCP,
166 with a mean decrease of $35 \mu\text{g}/\text{m}^3$, whereas the $\text{PM}_{2.5}$ anomalies increase in January
167 of 2015 ($33 \mu\text{g}/\text{m}^3$) and 2017 ($3 \mu\text{g}/\text{m}^3$) relative to the adjacent December anomaly
168 (Fig. S1 in the supporting information).



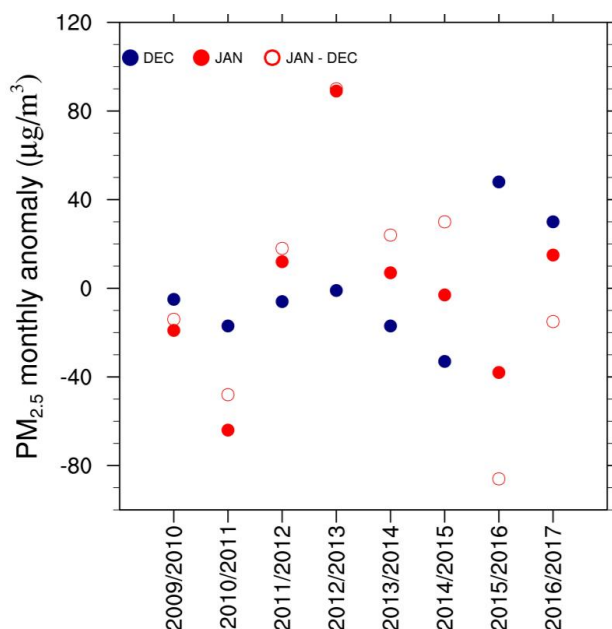
176 Figure 1. Monthly mean $\text{PM}_{2.5}$ concentration in December 2015, and the difference between the
177 anomaly of January 2016 (relative to January from 2015-2017) and December 2015 (relative to
178 December from 2014-2016)

179 3.2 $\text{PM}_{2.5}$ anomaly from long time series

180 To further test the robustness of the large drop of $\text{PM}_{2.5}$ from December 2015 to
181 January 2016, monthly mean anomaly of $\text{PM}_{2.5}$ relative to 2009-2017 over U.S.
182 Embassy Beijing is shown in Fig. 2. The $\text{PM}_{2.5}$ anomaly in December is generally
183 negative (i.e., low $\text{PM}_{2.5}$ concentration) from 2009-2014 except for a substantial
184 positive value of $48 \mu\text{g}/\text{m}^3$ in 2015. For the January $\text{PM}_{2.5}$ anomaly, the large positive
185 value in 2013 has been widely studied to investigate the mechanisms modulating the
186 severe haze events (Kajino et al., 2017; Shi et al., 2017; Han et al., 2016; Ye et al.,
187 2016). Looking at the difference between the January and December anomalies, the
188 exceptional difference between January 2016 and December 2015 stands out, with the
189 $\text{PM}_{2.5}$ concentration anomaly ($-38 \mu\text{g}/\text{m}^3$) in January 2016 showing a decrease of -86
190 $\mu\text{g}/\text{m}^3$ relative to the anomaly in December 2015 ($48 \mu\text{g}/\text{m}^3$), which is much more
191 negative than the difference in any other years and far more negative than the 99%
192 confidence interval value of $-66 \mu\text{g}/\text{m}^3$.



193 In addition to the single site of U.S. Embassy Beijing, two other data sets of air
194 pollution index (API; <http://datacenter.mep.gov.cn/>) and air quality index (AQI;
195 <http://www.pm25.in>) were combined to illustrate the robustness of the abnormal
196 difference between January and December PM_{2.5} over a larger spatial area in NCP
197 (black box in Fig. 1). Combining the API and AQI data allows anomaly to be
198 calculated relative to a longer period despite the short record of the AQI data. Similar
199 to Fig. 2, abnormally high concentration in December 2015 and low concentration in
200 January 2016 are also found in the API/AQI record (Fig. S2 in the supporting
201 information). As anthropogenic emissions such as NO_x, SO₂, and primary PM_{2.5}
202 have been steadily decreasing since 2011 (Liu et al., 2016; Wang et al., 2017), the
203 abnormally high PM_{2.5} concentration in December 2015 requires an explanation.
204 More interestingly, the emissions of SO₂ in January is usually higher than December
205 primarily due to a higher power demand, and this is the case for January 2016, with a
206 higher SO₂ concentration than December 2015 based on observed data
207 (<http://www.pm25.in>; not shown). Thus, what mechanism triggers the sharp decrease
208 of haze in January 2016 compared to December 2015 needs to be investigated.



209 Figure 2. Monthly mean anomaly of $PM_{2.5}$ in the adjacent December (solid blue) and
210 January (solid red) as well as the change (hollow red circle) from December to
211 January during 2009-2017 over US embassy Beijing. For December (January), the
212 anomaly is relative to 2009-2016 (2010-2017) eight-year respective monthly mean
213 value.

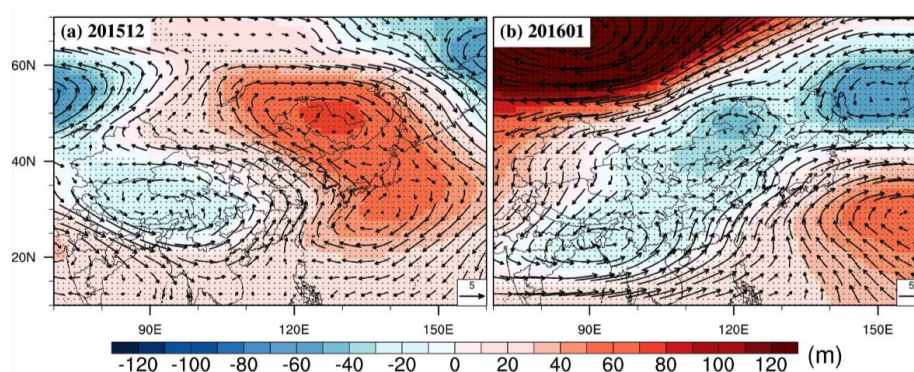
214 4. Mechanism modulating the high and low anomaly of $PM_{2.5}$

215 4.1 The effect of meteorological modulation

216 To determine if meteorological factors play a role in the anomalous December to
217 January change in $PM_{2.5}$, we first examined the mid-tropospheric circulation system
218 during December 2015 and January 2016. As shown in Fig. 3a for December 2015,
219 the northeastward shift of Siberian High and anticyclonic high pressure system in the
220 NCP reduced the northerly wind transporting cold air from Siberia to the NCP,
221 favoring the haze formation (Cai et al., 2017b; Chang et al., 2016). In January 2016
222 (Fig. 3b), a low pressure system dominates over the NCP area, enhancing the
223 northerly wind blowing from Siberia and relieving haze formation. An important



224 question here is whether the transition of the meteorological conditions from
225 December 2015 to January 2016 was influenced by climate variations on
226 seasonal-to-decadal time scales with some level of predictability.



227

228 Fig. 3 Anomaly of geopotential height and wind vector at 500 hPa. (The anomaly is
229 relative to 1987-2016). Stippled areas indicate geopotential height exceeding 90th
230 confidence interval.

231 4.2 Possible linkage with climate variability

232 From the Niño 3.4 index, defined as the 3-month running regional mean SST
233 anomaly over the tropical region (5 °S-5 °N, 170°-120°W) relative to 1951-2000
234 (Rayner et al., 2003), the El Niño signal reached a peak in December 2015, and
235 started to decay in January 2016. The development and decay of this El Niño event
236 and the associated change in circulation pattern have been well documented by Xue
237 and Kumar (2017). The 2015-2016 El Niño event is known as a super strong event
238 comparable to the other two super events during 1982/1983 and 1997/1998 (Ren et al.,
239 2017). Thus, it is appropriate to ask whether the circulation pattern in the NCP was
240 modulated by the development of a super El Niño. Motivated by this question, we
241 examined the super El Niño events in 1982/1983 and 1997/1998 based on Niño 3.4. In
242 1997/1998, the El Niño peaked in December 1997 and started to decay in January
243 1998, but in 1982/1983, the El Niño peaked in January 1983 and started to decay in

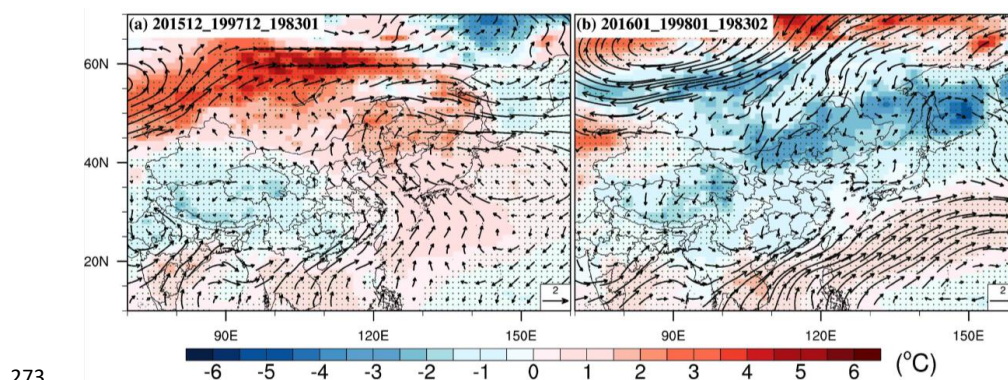


244 February 1983. The 500 hPa geopotential height anomalies during these four months
245 are shown in Fig. S3. Consistent with the anomalous circulation features in Fig. 3, an
246 anticyclonic circulation anomaly dominates over the NCP during the peak of the El
247 Niño (199712, 198301) while a cyclonic circulation anomaly prevails over the same
248 region when the El Niño started to decay (199801, 198302). To exclude this opposite
249 anomaly patterns as climatological features, we checked the 500 hPa anomalies in
250 December, January, and February during the past thirty years (1987-2016) but we
251 could not find similar opposite patterns in adjacent winter months during any other
252 years. This further hints at the possible linkage between the anomalous circulation
253 patterns and El Niño.

254 Since low-level wind has a larger influence on the formation of haze than
255 mid-tropospheric wind, the composited anomaly of 850 hPa wind vector and near
256 surface air temperature during the adjacent months of the super El Niño events
257 (January 1983, December 1997 and 2015 versus February 1983 and January 1998 and
258 2016) are shown in Fig. 4, while anomaly of near surface wind at 10-m is shown in
259 Fig. 5. These figures clearly depict opposite anomaly patterns in the NCP, showing
260 southerly anomaly (Fig. 5a; Fig. 6a) during the peak of the El Niño, and northerly
261 anomaly (Fig. 5b, Fig. 6b) during the start of the decay phase. The southerly wind
262 anomaly, abnormally warm near surface air temperature and stagnant weather
263 conditions over the NCP are indicative of weakened EAWM (Hui and Xiang, 2015)
264 partly related to the warmer air temperature over the northern plain and Siberia and
265 reduced pressure contrast between the Asian continent and the western Pacific Ocean,
266 favoring haze formation (Cai et al., 2017b; Li et al., 2018). In contrast, there is
267 enhanced northerly flow and more cold air advection (Fig. 5b, Fig. 6b) when El Niño
268 starts to decay. The low-level circulation patterns and near surface air temperature are
269 consistent with the seesaw changes of 500 hPa geopotential height from the peak of
270 the El Niño development to the beginning of its decay for all three super El Niño
271 events, highly implicative of a strong relationship between El Niño and haze



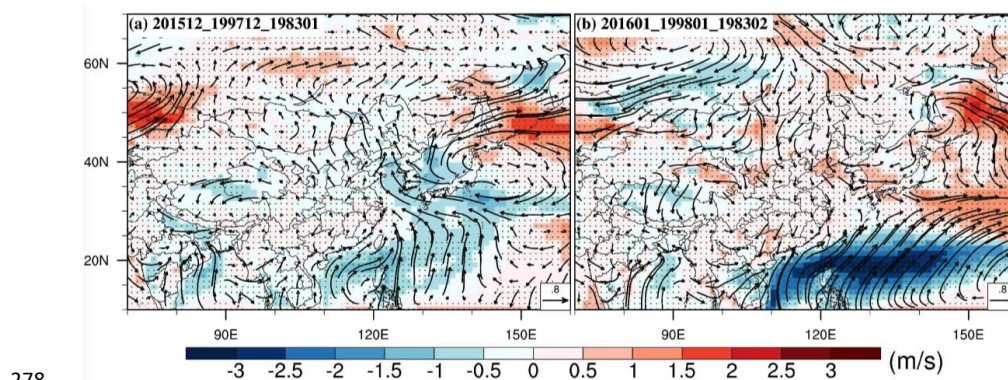
272 formation.



273

274 Fig. 4 850 hPa wind anomaly and 2-m air temperature anomaly (relative to
275 1987-2016). Stippled areas indicate 2-m air temperature exceeding 90th confidence
276 interval.

277



278

279 Fig. 5 Anomaly of 10-m wind vector with shading indicating the change in wind
280 speed (The anomaly is relative to 1987-2016). Stippled areas indicating exceedance of
281 90th confidence interval.

282 4.3 Sensitivities of PM_{2.5} to meteorological conditions

283 As shown in the above analyses, the meteorological conditions in December 2015,



284 December 1997, January 1983 exhibit a clear contrast with those of the following
 285 month. To demonstrate a connection between the meteorological conditions and haze
 286 formation, we used the WRF/CMAQ regional model to simulate haze for the three
 287 time periods under the same emissions, with a spatial resolution of 36 km by 36 km.
 288 The simulated meteorological conditions including near surface (2-meter) air
 289 temperature (T2) and specific humidity (Q2), 10-m wind speed (WS10) and direction
 290 (WD10) were evaluated using the NCEP Meteorological Assimilation Data Ingest
 291 System (MADIS; <https://madis.noaa.gov>) data on hourly time scale. Using the
 292 benchmark based on Emery et al. (2001), the meteorological parameters compared
 293 reasonably well with observations and mostly fall within or quite close to the
 294 benchmark, shown in the Table 1 below.

295 Table 1 Evaluation of WRF performance over North China (9 stations)*

NCP	201512				201601				Benchmark (Emery et al., 2001)			
	T2	Q2	WD10	WS10	T2	Q2	WD10	WS10	T2	Q2	WD10	WS10
Bias	0.31	0.24	19.25	0.96	0.07	0.25	1.48	0.92	< ±0.5	< ±1	< ±10	< ±0.5
Gross Error	2.31	0.63	88.36	1.57	2.30	0.54	85.39	1.79	< 2	< 2	< 30	/
RMSE	2.99	0.92	135.66	2.09	2.97	0.80	137.09	2.30	/	/	/	< 2

296 * T2: temperature at 2-meter with unit of °C

297 Q2: specific humidity with unit of g/kg

298 WD10: wind direction at 10-meter with unit of degrees

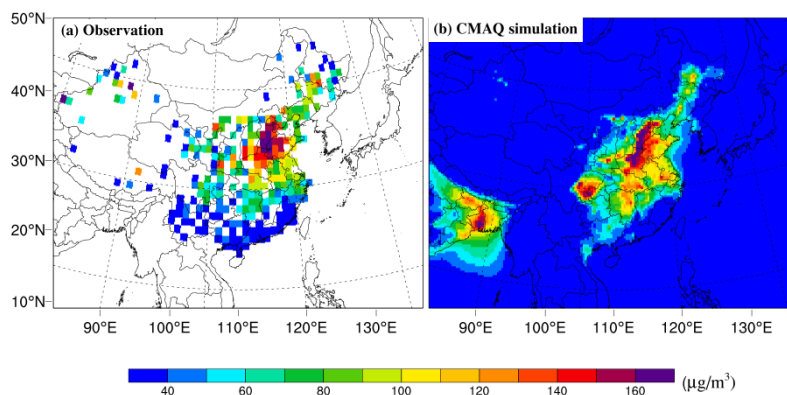
299 WS10: wind speed at 10-meter with unit of m/s

300

301 MCIP was used to prepare input for CMAQ. A code bug in MCIP 4.3 for
 302 processing land use information was found that affected the percentage of urban area
 303 (PURB), leading to low PM_{2.5} concentration in the simulations over urban areas (see
 304 the Supporting Information for more details). With the bug fix, the concentration of
 305 PM_{2.5} matches the observations well (Fig. 6). Statistical metrics such as mean
 306 fractional bias/error (MFB/MFE) were used to evaluate the simulation of PM_{2.5}, as
 307 recommended by US EPA (USEPA, 2007). Based on almost 200 observational sites in



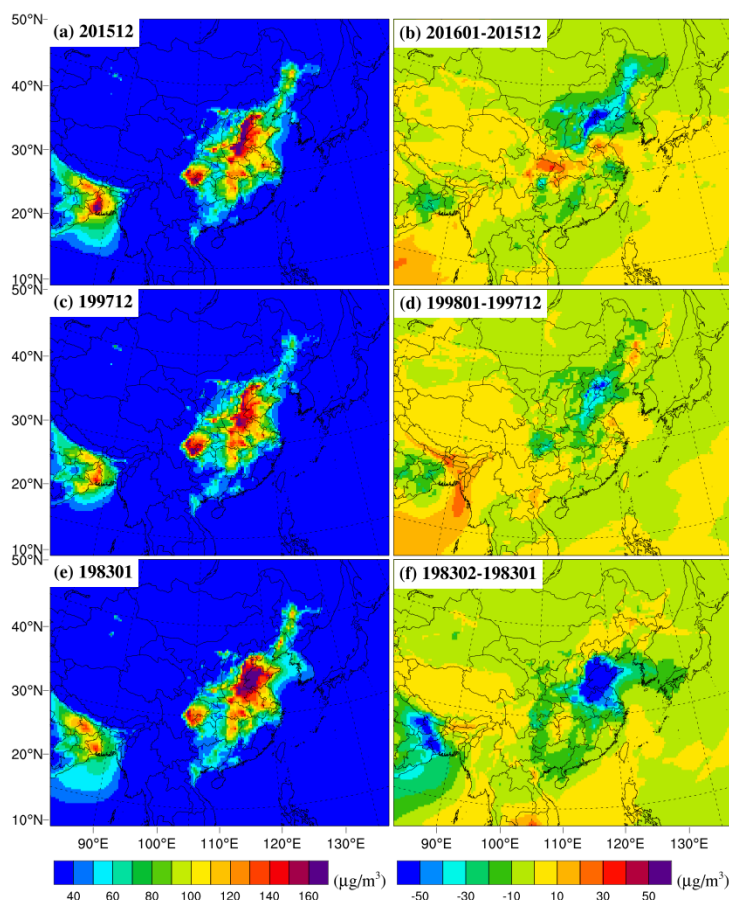
308 North China, the MFB/MFE of $PM_{2.5}$ from CMAQ is 1%/55% and 1%/56%,
309 respectively for December 2015 and January 2016, satisfying the benchmark of
310 50%/75% (USEPA, 2007).



311

312 Fig. 6. Spatial distributions of monthly mean $PM_{2.5}$ concentration in December
313 2015 for observations (a) and CMAQ simulation (b). Please note that the label bar
314 starts from $40 \mu\text{g}/\text{m}^3$ instead of 0 in order to make the comparison easily viewed.

315 Fig. 7 shows the spatial distribution of monthly mean $PM_{2.5}$ in December 2015
316 (Fig. 7a), December 1997 (Fig. 7c), January 1983 (Fig. 7e) and the differences
317 compared to the $PM_{2.5}$ in the following month. Although the same emissions at the
318 level of December 2015 were used across the simulations, the results clearly show
319 much higher monthly mean $PM_{2.5}$ in December 2015 (Fig. 7a), December 1997 (Fig.
320 7c), January 1983 (Fig. 7e) particularly over the NCP compared to the following
321 month (Figs. 7b,d,f), with mean reduction in the NCP of $30\text{-}50 \mu\text{g}/\text{m}^3$ or more. Hence
322 the modeling results further verified the effect of the meteorological conditions on the
323 seesaw $PM_{2.5}$ pattern.



324

325 Fig. 7 Monthly mean $PM_{2.5}$ during the three super El Niño events, i.e., December
326 2015 (a), December 1997 (c), January 1983 (e) and the differences of $PM_{2.5}$ compared
327 to the following month (b, d, and f)

328 4.4 Synthesis of the mechanism modulating the $PM_{2.5}$ variations

329 The different modulation effects of the development and decay phase of El Niño
330 on East Asian summer monsoon circulation have been noted in previous studies (Xue
331 et al., 2018; Yuan and Yang, 2012). For example, Xue et al. (2018) discussed a
332 mechanism for how developing El Niño in the summer modulates the intraseasonal
333 variation of the West Pacific Subtropical High (WPSH). They found that compared to
334 June and July, enhanced convection in August over the warm pool significantly

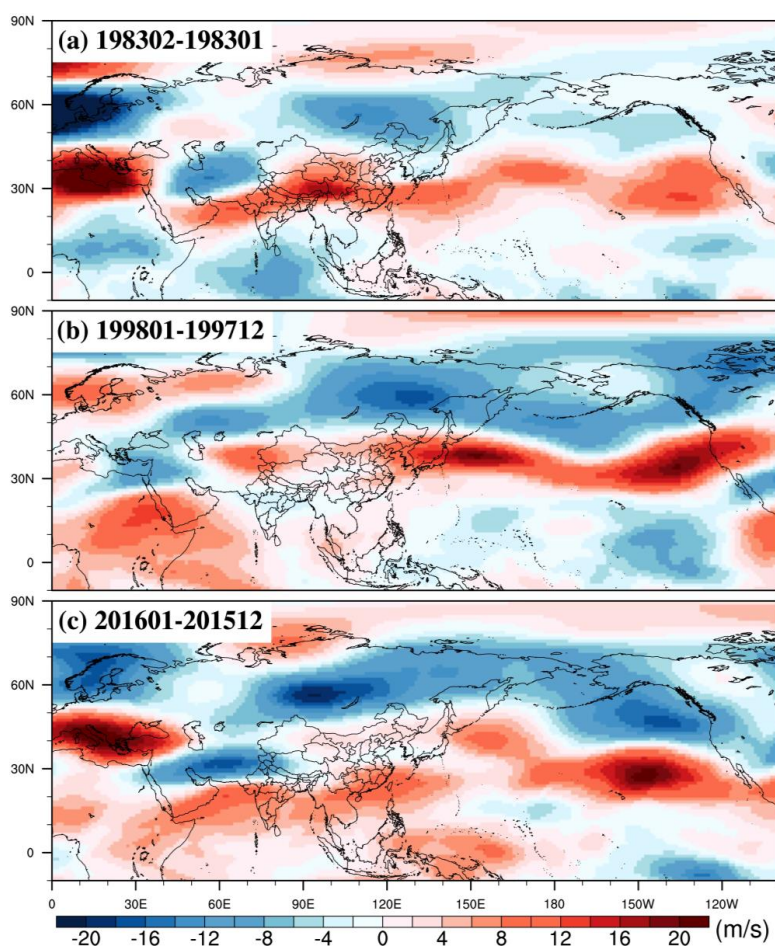


335 reduces the 500 hPa geopotential height and pushes the WPSH to retreat eastward
336 substantially. For intraseasonal variation in winter, Nie et al. (2016) found that the
337 change from warm anomaly in December 2015 to cold anomaly in January 2016 in
338 the NCP is possibly associated with the sudden shift of the Arctic Oscillation (AO)
339 from a positive phase to a negative phase in January 2016, which is dynamically
340 linked to super El Niño (Geng et al., 2017). The impact of the AO on the EAWM was
341 also demonstrated in December 2012 when the Siberian High and cold advection were
342 strong during the negative phase of the AO, but a transition of the AO to a positive
343 phase in January 2013 caused a sudden weakening of cold advection and increased
344 stagnation. The resulting severe haze in January 2013 has been widely discussed
345 previously (Cheng et al., 2017;Kajino et al., 2017).

346 The EAWM is closely related to winter haze conditions in the NCP. Cheung et al.
347 (2012) found that in general, the EAWM is enhanced (weakened) when the AO and
348 ENSO are in phase (out of phase). They also noted that a similar relationship at
349 sub-seasonal time scale may be further investigated considering the possibility of a
350 sharp reversal of the AO resulting from tropospheric–stratospheric interaction
351 (Baldwin and Dunkerton, 1999). To delve into the mechanism modulating the sudden
352 reversal of the AO from positive to negative phase during the decay of the mature
353 phase of El Niño, anomaly zonal wind changes at 200 hPa are shown in Fig. 8.
354 Climatologically (i.e., 1987-2016), the subtropical jet is centered around 35-40°N in
355 December and shift southward in January based on ERA-Interim (not shown). A clear
356 dipole feature of the sub-seasonal changes of anomaly zonal wind with negative
357 change north of 40°N indicates an obvious anomalous sub-seasonal southward shift of
358 the subtropical jet during the three El Niño events from its climatological
359 sub-seasonal shift. The subtropical jet shift has been confirmed by Geng et al. (2017)
360 using climate model simulations, showing phase transition of AO from positive to
361 negative in early January during super El Niño winter. The southward shift of the
362 upper tropospheric jet in January 2016 is likely associated with the weakened



363 stratospheric polar vortex and the subsequent negative phase of the AO (Fletcher and
364 Kushner, 2010; Bell et al., 2009), leading to more cold advection, enhanced EAWM,
365 and higher PBL height compared to the conditions during the peak of the El Niño with
366 lower PBL height (Fig. 9a). These changes in the meteorological conditions
367 associated with the changes in the El Niño development and AO phase shift and the
368 consequent changes in PM_{2.5} concentration are summarized schematically in Fig. 10.



369

370 Fig. 8 Sub-seasonal changes of anomaly of 200 hPa zonal wind (relative to 1987-2016)

371

during the start of the decay for three super El Niño events

372

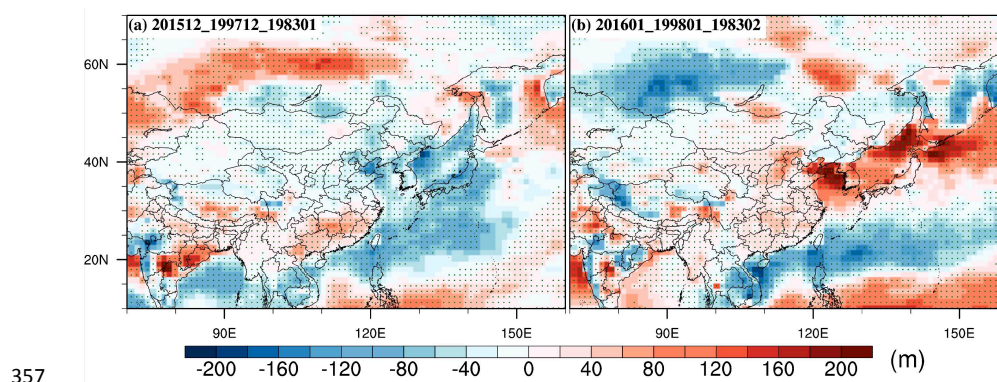


Fig. 9 Sub-seasonal changes of PBL height (relative to 1987-2016); stippled areas indicate exceedance of 90th confidence interval

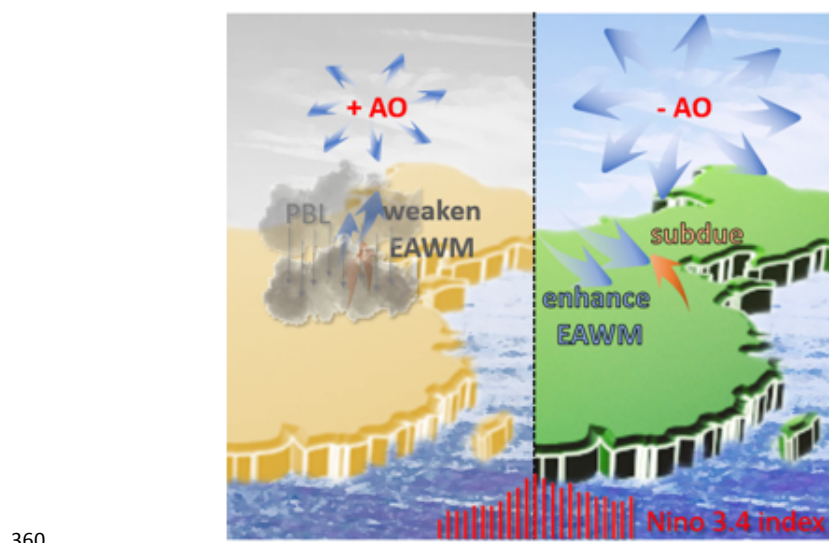


Fig. 10 Schematic of the modulation of El Niño and Arctic Oscillation on atmospheric circulation and haze in northern China



382 **Summary and discussions**

383 This study identifies a distinct seesaw feature of abnormally high and low monthly
384 mean $PM_{2.5}$ concentration in the two consecutive months of December 2015 and
385 January 2016, respectively, in the North China Plain. Accompanying the seesaw
386 features of $PM_{2.5}$ are opposite large scale circulation patterns with positive (negative)
387 anomaly of 500 hPa geopotential height and southerly (northerly) wind anomalies at
388 the low level (850 hPa) over the North China Plain during December 2015 (January
389 2016). The contrast in $PM_{2.5}$ between December 2015 and January 2016 is
390 significantly larger than the change from December to January between 2009 and
391 2017 recorded at US embassy Beijing.

392 As the modulation of meteorological conditions on $PM_{2.5}$ occurred during a strong
393 El Niño period, we explored the relationship between strong El Niño and $PM_{2.5}$. First,
394 using a regional climate/chemistry model WRF/CMAQ, we identified that all three
395 super El Niño events in the recent record (1982/83, 1997/98, and 2015/16) yield
396 similar seesaw modulation features of $PM_{2.5}$. Further analysis showed that the seesaw
397 $PM_{2.5}$ variations are modulated by the combined effect of El Niño and Arctic
398 Oscillation (AO). In December 2015, the mature phase of an extreme El Niño,
399 accompanied by a positive AO, weakened the EAWM, as indicated by a positive
400 anomaly of geopotential height at mid-troposphere (i.e., 500 hPa) and southerly wind
401 anomalies at the low level (i.e., 850 hPa) over the North China Plain (NCP), resulting
402 in reduced planetary boundary layer (PBL) height, abnormally warm temperature and
403 substantial haze accumulation during this period. In the following month (January
404 2016) when the El Niño began to decay, a sharp reversal of the AO from a positive
405 phase (in December 2015) to a negative phase triggered enhanced EAWM, inducing
406 cold advection and anomalous low-level northerly winds over the NCP that fostered
407 atmospheric dispersion and substantially reduced haze formation. This abrupt change
408 of the AO from a positive to a negative phase was robustly found for the other two
409 extreme El Niño events during the corresponding decay period (February 1983 and



410 January 1998) after the mature phase (January 1983 and December 1997). These
411 changes in circulation are likely associated with a southward shift of the upper
412 troposphere jet at 200 hPa and weakened stratospheric vortex during the decay phase
413 compared to the mature phase of El Niño. As the frequency of super El Niño like the
414 2015/16 event is projected to increase in the future (Cai et al., 2014; Cai et al., 2015),
415 the seesaw modulation of super El Niño and AO may become more frequent,
416 revealing vital information useful for policy makers dealing with air quality issues in
417 China.

418 Although we performed WRF-CMAQ simulations to demonstrate the impacts of
419 atmospheric circulation during three super El Niño events on haze, this study did not
420 isolate the general effect of El Niño and AO on haze formation. To address this
421 limitation, future studies will design Atmospheric Model Intercomparison Project
422 (AMIP) type scenarios, e.g., by running multi-ensemble members of scenarios with
423 global models such as Community Earth System Model (CESM) using different SSTs
424 over the Niño 3.4 area combined with dynamical downscaling using regional
425 climate/chemistry models such as WRF/CMAQ to elucidate the impact of El Niño
426 and AO on haze formation.

427 **Competing interests.** The authors declare that they have no conflict of interest.

428 **Acknowledgement.** This research was supported by grants from the National Natural Science
429 Foundation of China (91744208, 41705124), Shandong Provincial Natural Science Foundation,
430 China (ZR2017MD026) and the Fundamental Research Funds for the Central Universities
431 (201712006). PNNL is operated for DOE by Battelle Memorial Institute under contract
432 DE-AC05-76RL01830.

433

434 **References:**

435 Baldwin, M. P., and Dunkerton, T. J.: Propagation of the Arctic Oscillation from the stratosphere
436 to the troposphere, *J. Geophys. Res.*, 104, 30937-30946, 10.1029/1999JD900445, 1999.



- 437 Bell, C. J., Gray, L. J., Charlton-Perez, A. J., Joshi, M. M., and Scaife, A. A.: Stratospheric
438 Communication of El Niño Teleconnections to European Winter, *J. Clim.*, 22, 4083-4096,
439 10.1175/2009JCLI2717.1, 2009.
- 440 Byun, D., and Ching, J. K. S.: Science Algorithms of the EPA Models-3 CommunityMultiscale
441 Air Quality (CMAQ) Modeling System., U. S. Environmental Protection Agency, Office of Research
442 and Development, EPA, Washington, DC, 727, 1999.
- 443 Byun, D., and Schere, K. L.: Review of the governing equations, computational algorithms, and
444 other components of the models-3 Community Multiscale Air Quality (CMAQ) modeling system,
445 *Applied Mechanics Reviews*, 59, 51-77, 10.1115/1.2128636, 2006.
- 446 Cai, S. Y., Wang, Y. J., Zhao, B., Wang, S. X., Chang, X., and Hao, J. M.: The impact of the "Air
447 Pollution Prevention and Control Action Plan" on PM_{2.5} concentrations in Jing-Jin-Ji region during
448 2012-2020, *Sci Total Environ*, 580, 197-209, 10.1016/j.scitotenv.2016.11.188, 2017a.
- 449 Cai, W., Li, K., Liao, H., Wang, H., and Wu, L.: Weather conditions conducive to Beijing severe
450 haze more frequent under climate change, *Nature Clim. Change*, 7, 257-262, 10.1038/nclimate3249,
451 2017b.
- 452 Cai, W. J., Borlace, S., Lengaigne, M., van Rensch, P., Collins, M., Vecchi, G., Timmermann, A.,
453 Santoso, A., McPhaden, M. J., Wu, L. X., England, M. H., Wang, G. J., Guilyardi, E., and Jin, F. F.:
454 Increasing frequency of extreme El Niño events due to greenhouse warming, *Nature Climate Change*, 4,
455 111-116, 10.1038/nclimate2100, 2014.
- 456 Cai, W. J., Santoso, A., Wang, G. J., Yeh, S. W., An, S. I., Cobb, K. M., Collins, M., Guilyardi, E.,
457 Jin, F. F., Kug, J. S., Lengaigne, M., McPhaden, M. J., Takahashi, K., Timmermann, A., Vecchi, G.,
458 Watanabe, M., and Wu, L. X.: ENSO and greenhouse warming, *Nature Climate Change*, 5, 849-859,
459 10.1038/nclimate2743, 2015.
- 460 Chang, L., Xu, J., Tie, X., and Wu, J.: Impact of the 2015 El Niño event on winter air quality in
461 China, *Sci. Rep.*, 6, 34275, 10.1038/srep34275
- 462 <https://www.nature.com/articles/srep34275#supplementary-information>, 2016.
- 463 Chen, H., Lin, Y., Su, Q., and Cheng, L.: Spatial variation of multiple air pollutants and their
464 potential contributions to all-cause, respiratory, and cardiovascular mortality across China in 2015–
465 2016, *Atmos. Environ.*, 168, 23-35, <https://doi.org/10.1016/j.atmosenv.2017.09.006>, 2017.
- 466 Cheng, X. H., Sun, Z. A., Li, D. P., Xu, X. D., Jia, M. W., and Cheng, S. Y.: Short-term aerosol
467 radiative effects and their regional difference during heavy haze episodes in January 2013 in China,
468 *Atmos. Environ.*, 165, 248-263, 10.1016/j.atmosenv.2017.06.040, 2017.
- 469 Cheung, H. N., Zhou, W., Mok, H. Y., and Wu, M. C.: Relationship between Ural–Siberian
470 Blocking and the East Asian Winter Monsoon in Relation to the Arctic Oscillation and the El Niño–
471 Southern Oscillation, *J. Clim.*, 25, 4242-4257, 10.1175/JCLI-D-11-00225.1, 2012.
- 472 Dee, D. P., Uppala, S. M., Simmons, A. J., Berrisford, P., Poli, P., Kobayashi, S., Andrae, U.,
473 Balmaseda, M. A., Balsamo, G., Bauer, P., Bechtold, P., Beljaars, A. C. M., van de Berg, L., Bidlot, J.,
474 Bormann, N., Delsol, C., Dragani, R., Fuentes, M., Geer, A. J., Haimberger, L., Healy, S. B., Hersbach,
475 H., Hólm, E. V., Isaksen, I., Kållberg, P., Köhler, M., Matricardi, M., McNally, A. P., Monge-Sanz, B.,
476 Morcrette, J. J., Park, B. K., Peubey, C., de Rosnay, P., Tavolato, C., Thépaut, J. N., and Vitart, F.:
477 The ERA-Interim reanalysis: configuration and performance of the data assimilation system, *Q. J. Roy.
478 Meteor. Soc.*, 137, 553-597, 10.1002/qj.828, 2011.



- 479 Ding, A. J., Huang, X., Nie, W., Sun, J. N., Kerminen, V. M., Petäjä, T., Su, H., Cheng, Y. F., Yang,
480 X. Q., Wang, M. H., Chi, X. G., Wang, J. P., Virkkula, A., Guo, W. D., Yuan, J., Wang, S. Y., Zhang, R.
481 J., Wu, Y. F., Song, Y., Zhu, T., Zilitinkevich, S., Kulmala, M., and Fu, C. B.: Enhanced haze pollution
482 by black carbon in megacities in China, *Geophys. Res. Lett.*, 43, 2873-2879, 10.1002/2016GL067745,
483 2016.
- 484 Emery, C., Tai, E., and Yarwood, G.: Enhanced meteorological modeling and performance
485 evaluation for two Texas episodes, Prepared for the Texas Natural Resource Conservation Commission,
486 by ENVIRON International Corp, Novato, CA, 2001.
- 487 Fletcher, C. G., and Kushner, P. J.: The Role of Linear Interference in the Annular Mode Response
488 to Tropical SST Forcing, *J. Clim.*, 24, 778-794, 10.1175/2010JCLI3735.1, 2010.
- 489 Fu, X., Wang, S., Zhao, B., Xing, J., Cheng, Z., Liu, H., and Hao, J.: Emission inventory of
490 primary pollutants and chemical speciation in 2010 for the Yangtze River Delta region, China, *Atmos.*
491 *Environ.*, 70, 39-50, <https://doi.org/10.1016/j.atmosenv.2012.12.034>, 2013.
- 492 Gao, Y., Leung, L. R., Zhao, C., and Hagos, S.: Sensitivity of U.S. Summer Precipitation to Model
493 Resolution and Convective Parameterizations Across Gray Zone Resolutions, *J. Geophys. Res.*, 122,
494 2714-2733, 10.1002/2016jd025896, 2017.
- 495 Geng, X., Zhang, W., Stuecker, M. F., and Jin, F.-F.: Strong sub-seasonal wintertime cooling over
496 East Asia and Northern Europe associated with super El Niño events, *Sci. Rep.*, 7, 3770,
497 10.1038/s41598-017-03977-2, 2017.
- 498 Gunther, A., Karl, T., Harley, P., Wiedinmyer, C., Palmer, P. I., and Geron, C.: Estimates of
499 global terrestrial isoprene emissions using MEGAN (Model of Emissions of Gases and Aerosols from
500 Nature), *Atmos Chem Phys*, 6, 3181-3210, 2006.
- 501 Han, F., Xu, J., He, Y., Dang, H., Yang, X., and Meng, F.: Vertical structure of foggy haze over the
502 Beijing-Tianjin-Hebei area in January 2013, *Atmos. Environ.*, 139, 192-204,
503 10.1016/j.atmosenv.2016.05.030, 2016.
- 504 He, J., Gong, S., Yu, Y., Yu, L., Wu, L., Mao, H., Song, C., Zhao, S., Liu, H., Li, X., and Li, R.:
505 Air pollution characteristics and their relation to meteorological conditions during 2014–2015 in major
506 Chinese cities, *Environ. Pollut.*, 223, 484-496, <https://doi.org/10.1016/j.envpol.2017.01.050>, 2017.
- 507 Hui, G., and Xiang, L.: Influences of El Niño Southern Oscillation events on haze frequency in
508 eastern China during boreal winters, *Int. J. Climatol.*, 35, 2682-2688, 10.1002/joc.4133, 2015.
- 509 Jeong, J. I., and Park, R. J.: Winter monsoon variability and its impact on aerosol concentrations
510 in East Asia, *Environ. Pollut.*, 221, 285-292, <https://doi.org/10.1016/j.envpol.2016.11.075>, 2017.
- 511 Kajino, M., Ueda, H., Han, Z., Rei, K., Inomata, Y., and Kaku, H.: Synergy between air pollution
512 and urban meteorological changes through aerosol-radiation-diffusion feedback A case study of Beijing
513 in January 2013, *Atmos. Environ.*, 171, 98-110, 10.10164/j.atmosenv.2017.10.018, 2017.
- 514 Li, K., Liao, H., Cai, W., and Yang, Y.: Attribution of Anthropogenic Influence on Atmospheric
515 Patterns Conducive to Recent Most Severe Haze Over Eastern China, *Geophys. Res. Lett.*, in press.,
516 10.1002/2017GL076570, 2018.
- 517 Li, M., Liu, H., Geng, G., Hong, C., Liu, F., Song, Y., Tong, D., Zheng, B., Cui, H., Man, H.,
518 Zhang, Q., and He, K.: Anthropogenic emission inventories in China: a review, *National Science*
519 *Review*, 4, 834-866, 10.1093/nsr/nwx150, 2017.
- 520 Li, Q., Zhang, R., and Wang, Y.: Interannual variation of the wintertime fog–haze days across
521 central and eastern China and its relation with East Asian winter monsoon, *Int. J. Climatol.*, 36,



- 522 346-354, 10.1002/joc.4350, 2016.
- 523 Liang, F., Tian, L., Guo, Q., Westerdahl, D., Liu, Y., Jin, X., Li, G., and Pan, X.: Associations of
524 PM_{2.5} and Black Carbon with Hospital Emergency Room Visits during Heavy Haze Events: A Case
525 Study in Beijing, China, *Int. J. Environ. Res. Public Health*, 14, 725, 2017.
- 526 Liu, F., Zhang, Q., A., R. J. v. d., Zheng, B., Tong, D., Yan, L., Zheng, Y., and He, K.: Recent
527 reduction in NO_x emissions over China: synthesis of satellite observations and emission inventories,
528 *Environ. Res. Lett.*, 11, 114002, 2016.
- 529 Liu, Q., Sheng, L., Cao, Z., Diao, Y., Wang, W., and Zhou, Y.: Dual effects of the winter monsoon
530 on haze-fog variations in eastern China, *J. Geophys. Res.*, 122, 5857-5869, 10.1002/2016JD026296,
531 2017.
- 532 Nie, Y., Sun, L., Wang, D., and Li, D.: Possible Causes for the Sudden Drop of Air Temperature in
533 the Northern Hemisphere from Early- to Mid-Winter, *Meteorological Monthly*, 42, 1223-1229, 2016.
- 534 Otte, T. L., and Pleim, J. E.: The Meteorology-Chemistry Interface Processor (MCIP) for the
535 CMAQ modeling system: updates through MCIPv3.4.1, *Geosci. Model Dev.*, 3, 243-256,
536 10.5194/gmd-3-243-2010, 2010.
- 537 Qin, Y., and Xie, S. D.: Historical estimation of carbonaceous aerosol emissions from biomass
538 open burning in China for the period 1990–2005, *Environ. Pollut.*, 159, 3316-3323,
539 <https://doi.org/10.1016/j.envpol.2011.08.042>, 2011.
- 540 Rayner, N. A., Parker, D. E., Horton, E. B., Folland, C. K., Alexander, L. V., Rowell, D. P., Kent,
541 E. C., and Kaplan, A.: Global analyses of sea surface temperature, sea ice, and night marine air
542 temperature since the late nineteenth century, *J. Geophys. Res.*, 108, n/a-n/a, 10.1029/2002JD002670,
543 2003.
- 544 Ren, H. L., Wang, R., Zhai, P., Ding, Y., and Bo, L. U.: Upper-Ocean Dynamical Features and
545 Prediction of the Super El Nino in 2015/16: A Comparison with the Cases in 1982/83 and 1997/98,
546 *Journal of Meteorological Research*, 31, 278-294, 2017.
- 547 Saha, S., Moorthi, S., Wu, X., Wang, J., Nadiga, S., Tripp, P., Behringer, D., Hou, Y.-T., Chuang,
548 H.-y., Iredell, M., Ek, M., Meng, J., Yang, R., Mendez, M. P., van den Dool, H., Zhang, Q., Wang, W.,
549 Chen, M., and Becker, E.: The NCEP Climate Forecast System Version 2, *J. Clim.*, 27, 2185-2208,
550 10.1175/JCLI-D-12-00823.1, 2013.
- 551 Shi, Z., Li, J., Huang, L., Wang, P., Wu, L., Ying, Q., Zhang, H., Lu, L., Liu, X., Liao, H., and Hu,
552 J.: Source apportionment of fine particulate matter in China in 2013 using a source-oriented chemical
553 transport model, *Sci. Total Environ.*, 601, 1476-1487, 10.1016/j.scitotenv.2017.06.019, 2017.
- 554 Skamarock, W. C., Klemp, J. B., Dudhia, J., Gill, D. O., Barker, D. M., Duda, M. G., Huang, X.,
555 Wang, W., and Powers, J. G.: A description of the advanced research WRF version 3, NCAR Tech.
556 Note, NCAR/TN-475+STR, 8 pp., Natl. Cent. for Atmos. Res., Boulder, CO, USA, available at:
557 http://www.mmm.ucar.edu/wrf/users/docs/arw_v3.pdf, 2008, 2008.
- 558 Song, C., Wu, L., Xie, Y., He, J., Chen, X., Wang, T., Lin, Y., Jin, T., Wang, A., Liu, Y., Dai, Q.,
559 Liu, B., Wang, Y.-n., and Mao, H.: Air pollution in China: Status and spatiotemporal variations,
560 *Environ. Pollut.*, 227, 334-347, <https://doi.org/10.1016/j.envpol.2017.04.075>, 2017.
- 561 Tie, X., Huang, R.-J., Cao, J., Zhang, Q., Cheng, Y., Su, H., Chang, D., Pöschl, U., Hoffmann, T.,
562 Dusek, U., Li, G., Worsnop, D. R., and O'Dowd, C. D.: Severe Pollution in China Amplified by
563 Atmospheric Moisture, *Sci. Rep.*, 7, 15760, 10.1038/s41598-017-15909-1, 2017.
- 564 USEPA: Guidance on the Use of Models and Other Analyses for Demonstrating Attainment of Air



- 565 Quality Goals for Ozone, PM_{2.5} and Regional Haze, EPA-454/B-07e002, 2007.
- 566 Wang, J., Zhao, B., Wang, S., Yang, F., Xing, J., Morawska, L., Ding, A., Kulmala, M., Kerminen,
567 V.-M., Kujansuu, J., Wang, Z., Ding, D., Zhang, X., Wang, H., Tian, M., Petäjä, T., Jiang, J., and Hao,
568 J.: Particulate matter pollution over China and the effects of control policies, *Sci. Total Environ.*,
569 584-585, 426-447, <https://doi.org/10.1016/j.scitotenv.2017.01.027>, 2017.
- 570 Wang, S. X., and Zhang, C. Y.: Spatial and temporal distribution of air pollutant emissions from
571 open burning of crop residues in China, *Sciencepaper Onlin*, 3, 1-6, 2008.
- 572 Wang, S. X., Zhao, B., Cai, S. Y., Klimont, Z., Nielsen, C. P., Morikawa, T., Woo, J. H., Kim, Y.,
573 Fu, X., Xu, J. Y., Hao, J. M., and He, K. B.: Emission trends and mitigation options for air pollutants in
574 East Asia, *Atmos Chem Phys*, 14, 6571-6603, DOI 10.5194/acp-14-6571-2014, 2014.
- 575 Wu, G. X., Li, Z. Q., Fu, C. B., Zhang, X. Y., Zhang, R. Y., Zhang, R. H., Zhou, T. J., Li, J. P., Li,
576 J. D., Zhou, D. G., Wu, L., Zhou, L. T., He, B., and Huang, R. H.: Advances in studying interactions
577 between aerosols and monsoon in China, *Science China: Earth Sciences*, 45, 1609-1627,
578 10.1007/s11430-015-5198-z, 2015.
- 579 Xu, J., Chang, L., Yan, F., and He, J.: Role of climate anomalies on decadal variation in the
580 occurrence of wintertime haze in the Yangtze River Delta, China, *Sci. Total Environ.*, 599-600,
581 918-925, <https://doi.org/10.1016/j.scitotenv.2017.05.015>, 2017a.
- 582 Xu, L., Yu, J.-Y., Schnell, J. L., and Prather, M. J.: The seasonality and geographic dependence of
583 ENSO impacts on U.S. surface ozone variability, *Geophys. Res. Lett.*, 44, 3420-3428,
584 10.1002/2017GL073044, 2017b.
- 585 Xu, Q., Wang, S., Guo, Y., Wang, C., Huang, F., Li, X., Gao, Q., Wu, L., Tao, L., Guo, J., Wang,
586 W., and Guo, X.: Acute exposure to fine particulate matter and cardiovascular hospital emergency room
587 visits in Beijing, China, *Environ. Pollut.*, 220, 317-327, <https://doi.org/10.1016/j.envpol.2016.09.065>,
588 2017c.
- 589 Xue, F., Dong, X., and Fan, F. X.: Anomalous Western Pacific Subtropical High during El Nio
590 Developing Summer in Comparison with Decaying Summer, *Adv. Atmos. Sci.*, 35, 360-367,
591 10.1007/s00376-017-7046-x, 2018.
- 592 Xue, Y., and Kumar, A.: Evolution of the 2015/16 El Niño and historical perspective since 1979,
593 *SCIENCE CHINA Earth Sciences*, 60, 1572, doi:<https://doi.org/10.1007/s11430-016-0106-9>, 2017.
- 594 Yang, Y., Liao, H., and Lou, S.: Increase in winter haze over eastern China in recent decades:
595 Roles of variations in meteorological parameters and anthropogenic emissions, *J. Geophys. Res.*, 121,
596 13,050-013,065, 10.1002/2016JD025136, 2016.
- 597 Ye, X., Song, Y., Cai, X., and Zhang, H.: Study on the synoptic flow patterns and boundary layer
598 process of the severe haze events over the North China Plain in January 2013, *Atmos. Environ.*, 124,
599 129-145, 10.1016/j.atmosenv.2015.06.011, 2016.
- 600 Yin, Z., Wang, H., and Chen, H.: Understanding severe winter haze events in the North China
601 Plain in 2014: roles of climate anomalies, *Atmos. Chem. Phys.*, 17, 1641-1651,
602 10.5194/acp-17-1641-2017, 2017.
- 603 Yuan, Y., and Yang, S.: Impacts of Different Types of El Nino on the East Asian Climate: Focus
604 on ENSO Cycles, *J. Clim.*, 25, 7702-7722, 10.1175/jcli-d-11-00576.1, 2012.
- 605 Yuan, Y., Zhou, N., and Li, C.: Correlation between haze in North China and super El Niño
606 events., *Chinese J. Geophys*, 60, 11-20, 10.6038/cjg20170102, 2017.
- 607 Zhang, Q., Quan, J., Tie, X., Li, X., Liu, Q., Gao, Y., and Zhao, D.: Effects of meteorology and



- 608 secondary particle formation on visibility during heavy haze events in Beijing, China, *Sci. Total*
609 *Environ.*, 502, 578-584, <http://dx.doi.org/10.1016/j.scitotenv.2014.09.079>, 2015.
- 610 Zhang, Y., Ding, A., Mao, H., Nie, W., Zhou, D., Liu, L., Huang, X., and Fu, C.: Impact of
611 synoptic weather patterns and inter-decadal climate variability on air quality in the North China Plain
612 during 1980–2013, *Atmos. Environ.*, 124, 119-128, <https://doi.org/10.1016/j.atmosenv.2015.05.063>,
613 2016.
- 614 Zhang, Z., Gong, D., Mao, R., Kim, S.-J., Xu, J., Zhao, X., and Ma, Z.: Cause and predictability
615 for the severe haze pollution in downtown Beijing in November–December 2015, *Sci. Total Environ.*,
616 592, 627-638, <https://doi.org/10.1016/j.scitotenv.2017.03.009>, 2017.
- 617 Zhao, B., Wang, S. X., Liu, H., Xu, J. Y., Fu, K., Klimont, Z., Hao, J. M., He, K. B., Cofala, J.,
618 and Amann, M.: NO_x emissions in China: historical trends and future perspectives, *Atmos Chem Phys*,
619 13, 9869-9897, DOI 10.5194/acp-13-9869-2013, 2013a.
- 620 Zhao, B., Wang, S. X., Liu, H., Xu, J. Y., Fu, K., Klimont, Z., Hao, J. M., He, K. B., Cofala, J.,
621 and Amann, M.: NO_x emissions in China: historical trends and future perspectives, *Atmos.*
622 *Chem. Phys.*, 13, 9869-9897, 10.5194/acp-13-9869-2013, 2013b.
- 623 Zhao, B., Wang, S. X., Wang, J. D., Fu, J. S., Liu, T. H., Xu, J. Y., Fu, X., and Hao, J. M.: Impact
624 of national NO_x and SO₂ control policies on particulate matter pollution in China, *Atmos Environ*, 77,
625 453-463, DOI 10.1016/j.atmosenv.2013.05.012, 2013c.
- 626 Zhao, B., Wu, W. J., Wang, S. X., Xing, J., Chang, X., Liou, K. N., Jiang, J. H., Gu, Y., Jang, C.,
627 Fu, J. S., Zhu, Y., Wang, J. D., Lin, Y., and Hao, J. M.: A modeling study of the nonlinear response of
628 fine particles to air pollutant emissions in the Beijing-Tianjin-Hebei region, *Atmos Chem Phys*, 17,
629 12031-12050, DOI 10.5194/acp-17-12031-2017, 2017.
- 630 Zhao, S., Li, J., and Sun, C.: Decadal variability in the occurrence of wintertime haze in central
631 eastern China tied to the Pacific Decadal Oscillation, *Sci. Rep.*, 6, 27424, 10.1038/srep27424, 2016.

632